Dynamic Markers: Optimal control point configurations for homography and pose estimation

Raul Acuna[1] and Volker Willert[1]

Abstract— In this paper, we investigate in the influence of control points on the accuracy of space resection methods, e.g. used by a fiducial marker for pose estimation. More precisely, we propose a gradient descent optimization method to find optimal configurations of control points for the tasks of homography estimation and subsequent planar pose estimation from a number of $n \geq 4$ noisy point correspondences. We obtain optimal configurations by minimizing the first order perturbed solution of the direct linear transformation (DLT) algorithm which is equivalent to minimizing the condition number of the data matrix. This method guarantees point configurations which maximize the robustness of the DLT homography estimation against noise. Furthermore, a statistical evaluation is presented verifying that this optimal control point configurations even increase the performance of very accurate state of the art homography as well as pose estimation methods, like IPPE and EPnP, including the iterative minimization of the reprojection error MRE which is the most accurate algorithm. Finally, we provide a tradeoff between optimal configuration and the number of control points.

I. INTRODUCTION

The Perspective-n-Point (PnP) problem also known as space resection and the special case of planar pose estimation via homography estimation are some of the most researched topics in the fields of computer vision and photogrammetry. Even though the research in these areas has been wide, there is a surprising lack of information regarding the effect of the 3D control point configurations on the accuracy and robustness of the estimation methods.

As will be shown in Sec. II, it is clear from the literature, that the control point configurations are relevant and do influence accuracy as well as robustness of the pose estimates. However, these findings are rather general because they are based on hands-on experience and thus far only lead to some rules of thumb. Most obvious and widely accepted is, that increasing the number of control points increases the accuracy of the results in presence of noise. Further on, in several studies when simulations are performed to compare methods, great care is given to possible singular point configurations, such as non-centered data or near-planar cases which are singularities or degenerate cases for certain estimation methods.

A more thorough evaluation is given for the *normalized* DLT algorithm, whereas the normalization has already shown to improve the estimation because it is related to the condition number of the set of DLT equations [1]. The only
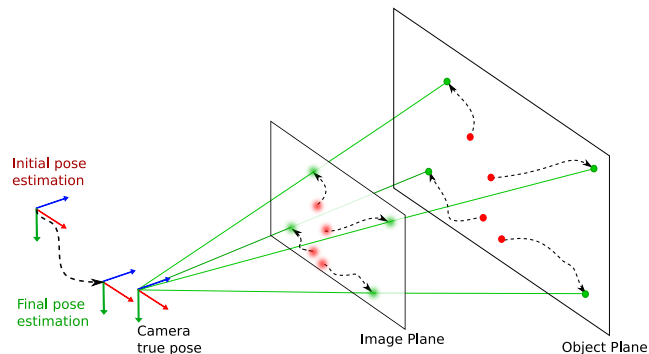
Fig. 1: The idea of a dynamic marker: The control points with known 3D coordinates on the object plane (marker) in arbitrary configuration (red) are moved towards optimal configurations (green) for pose estimation from these control points and their corresponding noisy projections on the image plane (blurry red and green). The control points' dynamics (12) is given by the gradient descent steps minimizing the optimization objective (11) that results in optimal pose estimations (from red to green) close to the true camera pose (black).

error analysis for homography estimation found so far by the authors in the literature presents a statistical analysis and simulations of the errors in the homography coefficients [2].

However, none of the above give an answer to the question: *Is there an optimal perspective-n-point configuration, which can increase the accuracy and robustness of space resection methods?*

If there is an optimal configuration, this question includes several follow-up questions: Is this optimal configuration dependent on the pose, or is there only one configuration that is optimal for all poses? What are the specifics of this/these configuration(s) in relation to absolute coordinates and relative distances between coordinates? Are there similarities between configurations that differ in the number of control points? When does an increase in number of points that are arbitrarily configured outperform the optimal configuration of a small number point set?

In this paper, we give an answer to all of these questions for planar control points by proposing an optimization objective to find optimal planar control point configurations. Figure 1 sketches the main idea of optimizing the proposed objective via a gradient descent approach and the stepwise improvement of the accuracy of the pose estimate starting from some initial control point configuration. Each descent step leads to a change in control point configuration and thus defines a dynamics for the control points that are placed on a planar visual fiducial marker (object plane), which we call a *dynamic marker*. This research could be relevant both for

those interested on the development of algorithms for PnP and space resection, as well for the community of fiducial marker designers.

The paper is structured as follows: In Sec. II, we classify pose estimation methods and summarize known findings about control point configurations. In Sec. III, we derive the optimization objective based on golden standard algorithms for pose estimation. In Sec. V, we describe the simulation results, and finally in Sec. VI, we discuss the results and give conclusions.

II. STATE OF THE ART

A. Brief history of space resection and PnP methods

Camera or space resection is a term used in the field of photogrammetry in which the spatial position and orientation of a photo is obtained by using image measurements of control points present on the photo. A similar concept comes from the computer vision community, where it is known as the Perspective-n-Point (PnP) problem. PnP can be considered an over-constrained (only for $n \geq 3$) and generic solution to the pose estimation problem from point correspondences. PnP methods can be classified into those which solve for a small and predefined number n of points, and those which can handle the general case. The minimal number of points to solve the PnP problem is three. Several solutions have been presented in the literature [3], which in general provide four solutions for non-collinear points. Thus, prior knowledge has to be included to choose the correct solution.

Since it has been proven that pose accuracy usually increases with the number of points [3], other PnP approaches that use more points ($n > 3$) are usually preferred. The general PnP methods can be broadly divided into whether they are iterative or non-iterative. Iterative approaches formulate the problem as a non-linear least-squares problem. They differ in the choice of the cost function to minimize, which is usually associated to an algebraic or geometric error. Some of the most important iterative methods in chronological order are: the **POSIT** algorithm [4], the **LHM** [5], the Procrustes PnP method or **PPnP** [6] and the global optimization method **SDP** [7].

Most iterative methods have the disadvantage that they return only a single pose solution, which might not be the true one. Most of them can only guarantee a local minimum, and the ones that find a global minimum remain computational intensive. The major limitation of iterative methods is that they are rather slow, neither convergence nor optimality can be guaranteed and a good initial guess is usually needed to converge to the right solution.

Non-iterative methods try to reformulate the problem so it may be solved by a potentially large equation system. However, early non-iterative solvers were also computational demanding and worse for a larger number of points. The first efficient and non-iterative $O(n)$ solution was **EPnP** [8], which was later improved by using an iterative method to increase accuracy. More recent approaches are based on polynomial solvers trying to achieve linear performance without the problems of EPnP and with higher accuracy. The first successful $O(n)$ method is the **DLS** [9], which uses a Cayley parametrization of the rotation, unfortunately with some degenerate cases.

Robust PnP or **RPnP** [10] is the first method that is more accurate when a low number of points is used $n \leq 5$, with similar accuracy to **LHM** but faster.

The **OPnP** (Optimal PnP) [11] is similar to DLS but a non-unit quaternion representation of the rotation is used. **UPnP** [12] is a linear non-iterative method that generalizes the solution into the NPnP (Non perspective n-point) problem. In contrast to OPnP the authors used normalized unit quaternions to represent rotations. More recently, in **optDLS** [13] a return to the Cayley rotation parametrization used on DLS is proposed, mentioning a simple trick to avoid the singularities, the method is three times faster than OPnP.

A special case of PnP is planar pose estimation, or PPE, which is a space resection problem that involves the process of recovering the relative pose of a plane with respect to a camera's coordinate frame from a single image measurement. A PPE problem can be solved by calculating the object-plane to image-plane homography transformation and then extracting the pose from the homography matrix. This is known as homography decomposition [14], [15], or by using a set of points in the plane as the measurement with a special case of the PnP methods (planar PnP). Some of the most important planar PnP methods are the iterative **RPP-SP** [16] and the more recent direct method **IPPE** [17]. In general planar PnP methods outperform the best homography decomposition methods when noise is present. Additionally, homography decomposition methods only provide a single solution in contrast to modern planar-PnP methods.

B. Homography estimation

The homography estimation is a key part of the homography decomposition methods and the IPPE algorithm. The standard linear algorithm for homography estimation is the Direct Linear Transform (DLT) [18], which was improved later in [19] using an orthogonalization step. For both methods the normalization of the measurements is a key step to improve the quality of the estimated homography [18]. However, the normalization has some disadvantages [20]: First, the normalization matrices are calculated from noisy measurements and are sensitive to outliers, and second, for a given measurement the noise affecting each point is independent of the others. However, in normalized measurements this independence is removed [2]. A method is proposed in [20] to overcome this problem by avoiding the normalization and using a Taubin estimator instead, obtaining similar results as the normalized one.

C. Control points configurations

It is pointed out in [8], [10] that 3D point configurations have an influence on the local minima of the PnP problem. In the RPnP paper [10] a broad classification of the control points configurations into three groups is presented. The classification is based on the rank of the matrix $\mathbf{M}^T\mathbf{M} \in \mathbb{R}^{3\times3}$, where $\mathbf{M} = [\mathbf{X}_1, \mathbf{X}_2, \ldots, \mathbf{X}_n]^T$, $\mathbf{X}_i$ is the 3D coordinate

of control point i and n is the amount of control points. The defined groups are: 1) Ordinary 3D case, when the $Rank(\mathbf{M}^T\mathbf{M}) = 3$ and the smallest singular value of $\mathbf{M}^T\mathbf{M}$ is different to zero. 2) Planar case, when the $Rank(\mathbf{M}^T\mathbf{M} = 2$ and 3) Quasi-singular case, when the $Rank(\mathbf{M}^T\mathbf{M}) = 3$ and the ratio of the smallest eigenvalue to the largest one is very small (< 0.05).

In the EPnP paper [8] it is shown that if the control points are taken from the *uncentered data* or the region where the image projections of the control points cover only a small part of the image, the stability of the compared methods greatly degrades. In RPnP it is elaborated that based on the previous classification this *uncentered data* is a configuration that lays between the *ordinary 3D case* and the *planar case*.

Some assumptions about the influence of the control points configurations are also present in the IPPE paper [17]. Through statistical evaluations the authors found out that the accuracy for the 4-point case decreases if the points are uniformly sampled from a given region. They circumvent this problem by selecting the corners of the region as the positions for the control points and then refer the reader to the Chen and Suter paper [2], were the analysis of the stability of the homography estimation to 1st order perturbations is presented. In this analysis it is clear that the error in homography estimate is dependent on the singular values of the $\mathbf{A}$ matrix in the DLT algorithm (see also next section).

Additionally, in [21], [22] evaluations are presented characterizing pose dependent offsets and uncertainty on the camera pose estimations. It is proven by simulations that different poses of the camera are more stable for the estimation process.

III. BASICS OF GOLDEN STANDARD ALGORITHMS FOR POSE ESTIMATION

Before we explain the optimization method for obtaining optimal point configurations, we shortly summarize the *golden standard* optimization methods for pose estimation from general and planar point configurations which are the minimization of the reprojection (geometric) error (MRE) for iterative methods and the minimization of the algebraic error for non-iterative methods via the DLT algorithm, respectively.

A. General point configuration for pose estimation

Given a 3D-2D point correspondence of i-th 3D control point p_i with world W coordinates $\mathbf{X}_i^W = [X_i^W, Y_i^W, Z_i^W]^T \in \mathbb{R}^3$ and its corresponding projection onto a planar calibrated camera[1] with normalized image coordinates $\mathbf{x}_i = [x_i, y_i]^T \in \mathbb{R}^2$ the relation between these points is given by the relative pose[2] $g = (\mathbf{R}, \mathbf{T})$ (Euclidean transformation) between world W and camera C frame $\mathbf{X}_i^C = \mathbf{R}\mathbf{X}_i^W + \mathbf{T}$ followed by a projection π with $\mathbf{x}_i = \pi(\mathbf{X}_i^C) = [X_i^C/Z_i^C, Y_i^C/Z_i^C]^T$.

This leads to the relation:

$$\mathbf{x}_i = \pi(\mathbf{X}_i^C) = \pi(\mathbf{R}\mathbf{X}_i^W + \mathbf{T}). \tag{1}$$

Including additive noise $\boldsymbol{\varepsilon}_i = [\varepsilon_i, \zeta_i]^T$ on the error-free image coordinates $\mathbf{x}_i$ we get noisy measurements of the image coordinates $\tilde{\mathbf{x}}_i = \mathbf{x}_i + \boldsymbol{\varepsilon}_i$. Thus, we can solve for the reprojection error $\|\boldsymbol{\varepsilon}_i\|_2^2 = \|\tilde{\mathbf{x}}_i - \mathbf{x}_i\|_2^2$ of each point which is a squared 2-norm. Minimizing the squared 2-norm of all points for the optimal pose $(\hat{\mathbf{R}}, \hat{\mathbf{T}})$ leads to the following least-squares estimator

$$(\hat{\mathbf{R}}, \hat{\mathbf{T}}) = \mathrm{argmin}_{\mathbf{R}, \mathbf{T}} \sum_{i=1}^n \|\boldsymbol{\varepsilon}_i\|_2^2, \quad n \geq 3. \tag{2}$$

Iterative gradient descent optimization of (2) leads to the most accurate pose estimation results in the literature so far, also for planar point configurations.

B. Planar point configuration for pose estimation

If the control points $\mathbf{X}_i^W$ are all on a plane P, we can define a 2D subspace in the 3D world with coordinates[3] $\mathbf{X}_i^P = [X_i^P, Y_i^P]^T \in \mathbb{R}^2$. Plugging the planar constraint in equation (1), extending to homogeneous coordinates and rearranging the equation, leads to a homography mapping

$$\mathbf{X}_i^C = Z_i^C \bar{\mathbf{x}}_i = [\mathbf{r}_1, \mathbf{r}_2, \mathbf{T}] \bar{\mathbf{X}}_i^P = \mathbf{H}\bar{\mathbf{X}}_i^P. \tag{3}$$

Eliminating Z_i^C, we get $\bar{\mathbf{x}}_i \times \mathbf{H}\bar{\mathbf{X}}_i^P = 0$, where each point correspondence $\{\mathbf{x}_i, \mathbf{X}_i^P\}$ produces two linearly independent equations

$$\mathbf{A}_i\mathbf{h} = \begin{bmatrix} \mathbf{O} & -(\bar{\mathbf{X}}_i^P)^T & y_i(\bar{\mathbf{X}}_i^P)^T \\ (\bar{\mathbf{X}}_i^P)^T & \mathbf{O} & x_i(\bar{\mathbf{X}}_i^P)^T \end{bmatrix} \begin{bmatrix} \mathbf{r}_1 \\ \mathbf{r}_2 \\ \mathbf{T} \end{bmatrix} = \mathbf{0}, \tag{4}$$

with $\mathbf{h} = [\mathbf{r}_1^T, \mathbf{r}_2^T, \mathbf{T}^T]^T \in \mathbb{R}^9$ and $\mathbf{A}_i \in \mathbb{R}^{2 \times 9}$.

Again, assuming noisy measurements of the image coordinates $\tilde{\mathbf{x}}_i = \mathbf{x}_i + \boldsymbol{\varepsilon}_i$, we get noisy matrices

$$\tilde{\mathbf{A}}_i = \begin{bmatrix} \mathbf{O} & -(\bar{\mathbf{X}}_i^P)^T & \tilde{y}_i(\bar{\mathbf{X}}_i^P)^T \\ (\bar{\mathbf{X}}_i^P)^T & \mathbf{O} & \tilde{x}_i(\bar{\mathbf{X}}_i^P)^T \end{bmatrix} = \mathbf{A}_i + \mathbf{E}_i \tag{5}$$

$$= \begin{bmatrix} \mathbf{O} & -(\bar{\mathbf{X}}_i^P)^T & y_i(\bar{\mathbf{X}}_i^P)^T \\ (\bar{\mathbf{X}}_i^P)^T & \mathbf{O} & x_i(\bar{\mathbf{X}}_i^P)^T \end{bmatrix}$$

$$+ \begin{bmatrix} \mathbf{O} & \mathbf{O} & \zeta_i(\bar{\mathbf{X}}_i^P)^T \\ \mathbf{O} & \mathbf{O} & \varepsilon_i(\bar{\mathbf{X}}_i^P)^T \end{bmatrix}. \tag{6}$$

From $\tilde{\mathbf{A}}_i\mathbf{h} = (\mathbf{A}_i + \mathbf{E}_i)\mathbf{h}$ we can solve for the algebraic error $\|\mathbf{E}_i\mathbf{h}\|_2^2 = \|(\tilde{\mathbf{A}}_i - \mathbf{A}_i)\mathbf{h}\|_2^2 = \|\tilde{\mathbf{A}}_i\mathbf{h}\|_2^2$ of each point, because $\mathbf{A}_i\mathbf{h} = \mathbf{0}$ holds. Minimizing the squared 2-norm of all points for the optimal homography $\hat{\mathbf{h}}$ leads to the following least-squares estimator

$$\hat{\mathbf{h}} = \mathrm{argmin}_{\mathbf{h}} \sum_{i=1}^n \|\mathbf{E}_i\mathbf{h}\|_2^2, \quad s.t. \ \|\mathbf{h}\| = 1, \quad n \geq 4. \tag{7}$$

Since $\mathbf{h}$ contains 9 entries, but is defined only up to scale the total number of degrees of freedom is 8. Thus, the additional constraint $\|\mathbf{h}\| = 1$ is included to solve the optimization.

---

[1]Assuming the calibration matrix $\mathbf{K} \in \mathbb{R}^{3 \times 3}$ to be known, the homogeneous image coordinates in pixel $\bar{\mathbf{x}}_i' = [x_i', y_i', 1]^T$ can be transformed to homogeneous normalized image coordinates in metric units $\bar{\mathbf{x}}_i = \mathbf{K}^{-1}\bar{\mathbf{x}}_i'$.

[2]The rotation matrix is given by: $\mathbf{R} = [\mathbf{r}_1, \mathbf{r}_2, \mathbf{r}_3] \in \mathbb{R}^{3 \times 3} | \mathbf{R}^T\mathbf{R} = \mathbf{I}, |\mathbf{R}| = 1$.

[3]Corresponding homogeneous coordinates are $\bar{\mathbf{X}}_i^P = [X_i^P, Y_i^P, 1]^T \in \mathbb{R}^3$.

Now, stacking all $\{\tilde{\mathbf{A}}_i\}$ and $\{\mathbf{E}_i\}$ as $\tilde{\mathbf{A}} = [\tilde{\mathbf{A}}_1^T, \ldots, \tilde{\mathbf{A}}_n^T]^T \in \mathbb{R}^{2n \times 9}$ and $\mathbf{E} = [\mathbf{E}_1^T, \ldots, \mathbf{E}_n^T]^T \in \mathbb{R}^{2n \times 9}$ respectively, we arrive at solving the noisy homogeneous linear equation system

$$\tilde{\mathbf{A}}\mathbf{h} = \mathbf{E}\mathbf{h}. \tag{8}$$

The solution of (8) is equivalent to the solution of (7) and is given by the DLT algorithm applying a singular value decomposition (SVD) of $\tilde{\mathbf{A}} = \tilde{\mathbf{U}}\tilde{\mathbf{S}}\tilde{\mathbf{V}}^T$, whereas $\hat{\mathbf{h}} = \tilde{\mathbf{v}}_9$ with $\tilde{\mathbf{v}}_9$ being the right singular vector of $\tilde{\mathbf{A}}$, associated with the least singular value $\tilde{s}_9$. Usually, an additional normalization step of the coordinates of the control points and its projections is performed leading to the normalized DLT algorithm which is the golden standard for non-iterative pose estimation, because it is very easy to handle and serves as a basis for other non-iterative as well as iterative pose estimation methods.

IV. OPTIMAL POINTS CONFIGURATION FOR POSE ESTIMATION

In order to find an optimal control points configuration in the field of view of a camera for estimating the pose of the same camera, we need a proper optimization criterion. In the following, we propose an optimization criterion that is optimal for planar pose estimation using the (normalized) DLT algorithm. We start with availing ourselfs of perturbation theory applied to singular value decomposition of noisy matrices [23] and have a look at the first order perturbation expansion for the perturbed solution of the DLT algorithm, given in [2], which is

$$\hat{\mathbf{h}} = \tilde{\mathbf{v}}_9 = \mathbf{v}_9 - \sum_{k=1}^{8} \frac{\mathbf{u}_k^T \mathbf{E} \mathbf{v}_9}{s_k} \mathbf{v}_k. \tag{9}$$

Equation (9) clearly shows that the optimal solution for the homography that equals the right singular vector of the unperturbed matrix $\mathbf{A}$, associated with the least singular value[4] $s_9 = 0$, is perturbed by the second term in (9). The second term is a weighted sum of the first eight optimal right singular vectors $\mathbf{v}_k$, whereas the weights $\mathbf{u}_k^T \mathbf{E} \mathbf{v}_9 / s_k$ are the influence of the measurement errors $\mathbf{E}$ on the unperturbed solution $\mathbf{v}_9$ along the different k dimensions of the model space. The presence of very small s_k in the denominator can give us very large weights for the corresponding model space basis vector $\mathbf{v}_k$ and dominate the error. Hence, small singular values s_k cause the estimation $\hat{\mathbf{h}}$ to be extremely sensitive to small amounts of noise in the data and correlates with the singular value spectrum[5] $(s_1 - s_8)$ as follows: The smaller the singular value spectrum, the less perturbed the estimation is. It is also well known, that the condition number of a matrix with respect to the 2-norm is given by the ratio between the largest and, in our case, second-smallest singular value [24]

$$c(\mathbf{A}) = \|\mathbf{A}\|_2 \|\mathbf{A}^{-1}\|_2 = \frac{s_{max}}{s_{min}} = \frac{s_1}{s_8}, \tag{10}$$

[4]The singular values are arranged in descending order: $s_1 \geq s_2 \geq \cdots \geq s_8 \geq s_9 = 0$.

[5]Here, the singular value spectrum between the first and second-last singular value is relevant, because $s_9 = 0$ holds.
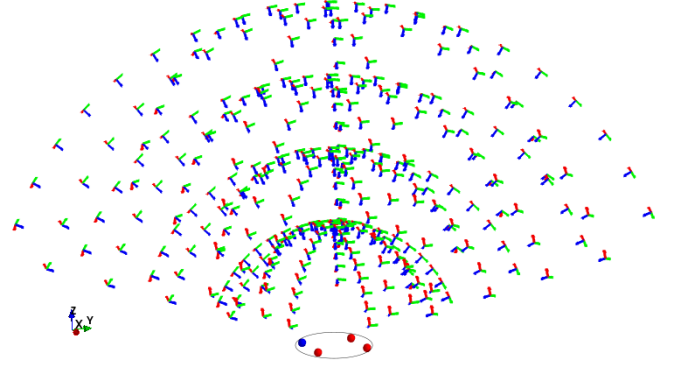

Fig. 2: Distribution of 400 camera poses used in simulations. A limiting circular plane with n control points inside is displayed at the bottom. The cameras are distributed evenly on spheres of evenly sampled radii, each one looking at the center of the circular plane. Only camera poses which had all limits of the circular plane in field of view were used.

which is minimal if the singular value spectrum is minimal. The normalization of the control points and its projections which leads to the normalized DLT algorithm has already shown to improve the condition of matrix $\mathbf{A}$ [1]. Thus, we simply try to minimize the condition number c of matrix $\mathbf{A}$ with respect to all n control points $\{\mathbf{X}_i^P\}$ like follows:

$$\{\hat{\mathbf{X}}_i^P\} = \operatorname{argmin}_{\{\mathbf{X}_i^P\}} c\left(\mathbf{A}(\{\mathbf{X}_i^P\})\right). \tag{11}$$

Optimization of (11) is realized with a gradient descent minimization, whereas for calculation of the gradient vector we use automatic differentiation[6] [26]. This leads to the final discrete control points dynamics

$$\mathbf{X}_i^P(t+1) = \mathbf{X}_i^P(t) - \alpha(t)\nabla c\left(\mathbf{A}\left(\mathbf{X}_i^P(t)\right)\right), \tag{12}$$

for each iteration t and stepsize $\alpha(t)$, which is adapted using SuperSAB [27]. The control points dynamics can now be used to find optimal control point configurations for pose estimation from planar markers. This is what we call *dynamic markers*.

V. SIMULATION RESULTS

Our simulation setup is based on a perspective camera model and a circular planar visual marker of radius $r = 0.15$ meters on the plane $Z_i^W = 0$ centered in the origin $\mathbf{X}_o^W = [0, 0, 0]^T$ of world coordinates. A set of control points are defined inside the limits of this circular plane, which are then projected onto the camera image[7].

A uniform distribution of 400 camera poses is defined around the circular plane as displayed in Fig. 2.

To evaluate the improvement of the gradient descent optimization, we consider the optimization objective, which is the condition number (10) at each iteration t, given by $c(\mathbf{A}(t))$ in the DLT algorithm. To evaluate the effect of the optimization (11) on the underlying homography estimate $\hat{\mathbf{H}}(t)$ using a given set of n control points $\{\mathbf{X}_i^P\}(t)$, we rely

[6]For implementation, we used *autograd* [25].

[7]Camera parameters: size $640 \times 480 [pixel^2]$, intrinsic parameters $\mathbf{K} = [800, 0, 320; 0, 800, 240; 0, 0, 1]$.

on the reprojection error $HE(\hat{\mathbf{H}}(t))$ induced by the estimated homography $\hat{\mathbf{H}}(t)$ given by

$$HE\left(\hat{\mathbf{H}}(t)\right) = \frac{1}{M}\sum_{j=1}^{M}\|\mathbf{x}_j(t) - \pi\left(\hat{\mathbf{H}}(t)\overline{\mathbf{X}}_j^P(t)\right)\|_2^2, \quad (13)$$

for a fixed set of M validation control points $\{\mathbf{X}_j^P\} \notin \{\mathbf{X}_i^P\}(t)$ that are evenly distributed on the object plane covering an area larger than the limits of the circle. Thus, it is possible to measure how good $\hat{\mathbf{H}}(t)$ is able to represent the true homography $\mathbf{H}$ beyond the space of the control points.

Each simulation for a given camera pose is then performed in the following way: 1) An initial random n-point set $\{\mathbf{X}_i^P\}(t_{start})$ is defined inside the circular plane 2) For each iteration step t an improved set of control points $\{\mathbf{X}_i^P\}(t)$ is obtained by (12) and projected to image coordinates $\{\mathbf{x}_i\}(t)$ using the true camera pose $\mathbf{R}, \mathbf{T}$ and calibration matrix $\mathbf{K}$. Then, the correspondences $\{\mathbf{x}_i(t), \mathbf{X}_i^P(t)\}$ are used to calculate $\mathbf{A}(t)$ and $c(\mathbf{A}(t))$. 3) For each t a statistically meaningful measure of the homography estimation robustness against noise is desired. Thus, 1000 runs of the homography estimation using the DLT algorithm were performed[8]. In each of this runs Gaussian noise with standard deviation σ_G was added to the image coordinates for the simulation of real camera measurements $\{\tilde{\mathbf{x}}_i\}(t)$. Finally, the error $HE\left(\hat{\mathbf{H}}(t)\right)$ is calculated in each run and the average $\mu\left(HE\left(\hat{\mathbf{H}}(t)\right)\right)$ and standard deviation $\sigma\left(HE\left(\hat{\mathbf{H}}(t)\right)\right)$ of this error for all runs is computed.

As illustration of the gradient minimization process an example case of a simulation in a fronto-parallel camera pose for a 4-point configuration is presented. A Gaussian noise of $\sigma_G = 4$ pixel is added to image coordinates for the homography estimation runs. In Fig. 3 the initial object and image point configurations are shown. The movement of points present two main characteristics: first, they are driven to separate from each other, and second, they tend to equalize distance to each other in object space. This results in stable square-like shaped configurations on average.

The evolution of $c(\mathbf{A}(t))$ as well as $\mu\left(HE\left(\hat{\mathbf{H}}(t)\right)\right)$ and $\sigma\left(HE\left(\hat{\mathbf{H}}(t)\right)\right)$ is presented in Fig. 4. The condition number decreases drastically in the first iterations of the gradient descent, and by doing so the mean and standard deviation of $HE\left(\hat{\mathbf{H}}(t)\right)$ is also reduced. With more iterations both metrics slowly and smoothly converge to a minimum stable value.

This first result in itself is highly representative as it proves that some point configurations increase the accuracy of homography estimation methods as well as the robustness to noise and it is also possible to obtain optimal point configurations.

Motivated by the homography results, it was of interest to test if these point configurations could improve as well the accuracy of pose estimation algorithms. Thus, three
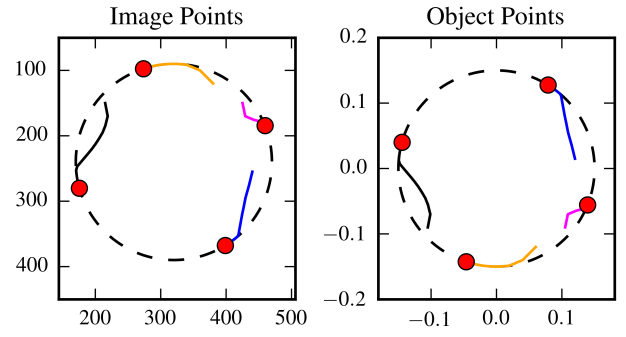

Fig. 3: (Fronto-Parallel). Movement of control points (colored lines) in image $\mathbf{x}_i(t)$ and object coordinates $\mathbf{X}_i^P(t)$ during gradient descent optimization for the fronto-parallel camera configuration until the final optimal configuration $\{\mathbf{X}_i^P\}(t_{end})$ (red dots) limited by the circle (dotted black line).
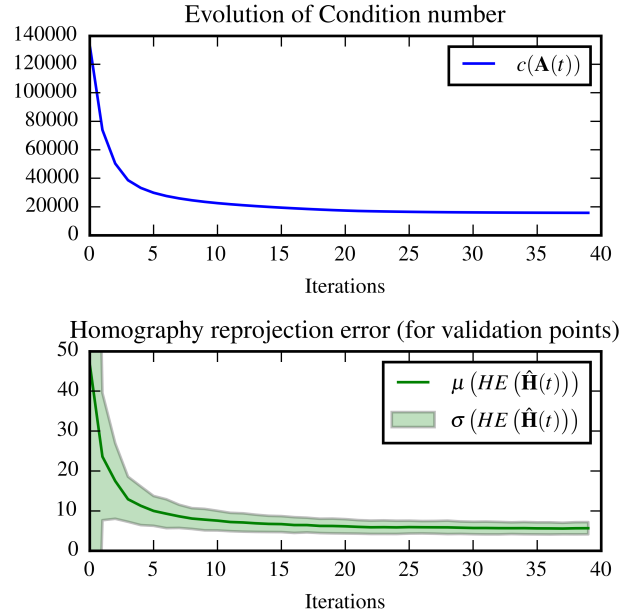

Fig. 4: (Fronto-Parallel). Evolution of the condition number $c(\mathbf{A}(t))$ as well as mean and standard deviation of the homography reprojection error $HE\left(\hat{\mathbf{H}}(t)\right)$ during gradient descent.

different pose estimation algorithms[9] were run at each iteration t of the optimization process, namely: 1) a non-iterative PnP method **EPnP** [8], 2) a planar pose estimation method **IPPE** [17], and 3) a fully iterative one based on the Levenberg-Marquardt optimization denoted as **LM**.

As in similar works [8], [17], we denote $\left(\hat{\mathbf{R}}(t), \hat{\mathbf{T}}(t)\right)$ as the estimated rotation and translation for a given camera pose at iteration t and by $(\mathbf{R}, \mathbf{T})$ the true rotation and translation. The error metrics for pose estimation are defined as follows:

- $RE(\hat{\mathbf{R}}(t))$ is the rotational error (in degrees) defined as the minimal rotation needed to align $\hat{\mathbf{R}}(t)$ to $\mathbf{R}$. It is obtained from the axis-angle representation of $\hat{\mathbf{R}}(t)^T\mathbf{R}$.
- $TE(\hat{\mathbf{T}}(t)) = \|\hat{\mathbf{T}}(t) - \mathbf{T}\|_2/\|\mathbf{T}\|_2 \times 100\%$ is the relative

---

[8]The homography estimation method presented in [19] and the gradient based one of OpenCV were also tested. The results almost do not differ for low point configurations to the DLT, so it was the chosen one for the experiments.

[9]For the EPnP and LM methods, the OpenCV implementations were used, and for IPPE the Python implementation provided by the author's github repository.
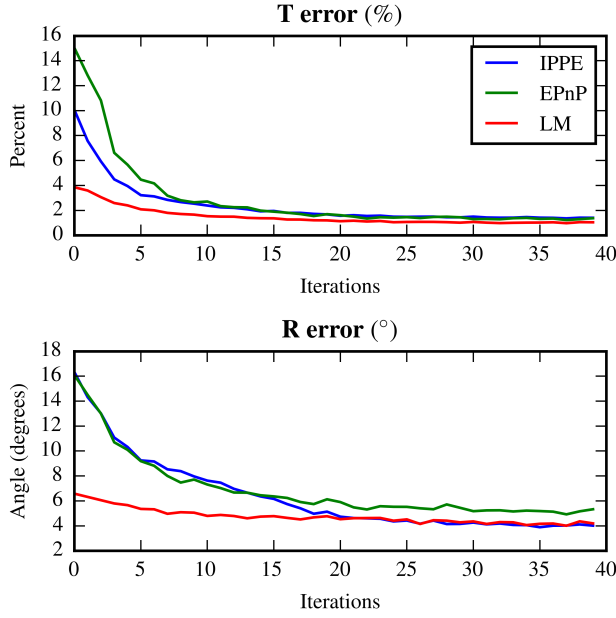
Fig. 5: (Fronto-Parallel). Comparison of the mean errors for the selected PnP estimation methods during the iterations of the optimization process.
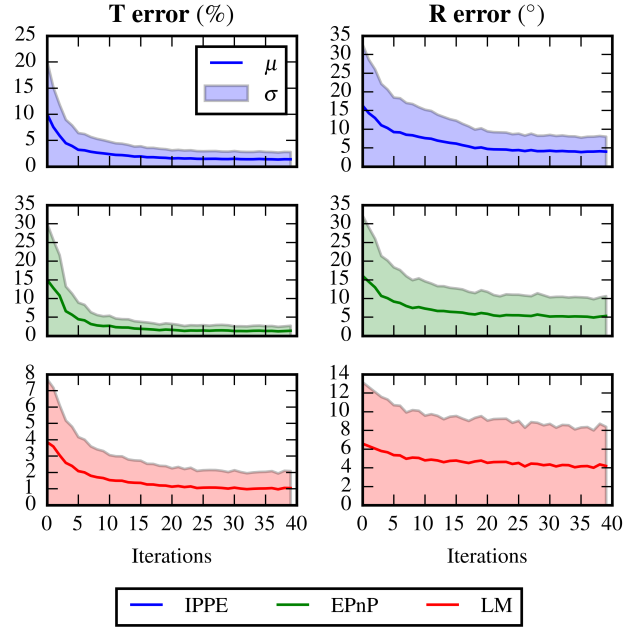

Fig. 6: (Fronto-Parallel). Detailed view of the standard deviation of each method represented by the filled colored areas.

Fig. 7: (Inclined). Movement of control points in image and object coordinates during gradient descent for the inclined camera configuration.

error in translation.

Similar to the homography simulation, for each iteration t, 1000 runs of the pose estimation with noisy correspondences for each of the PnP methods were performed. Then, the mean and standard deviation of RE and TE for the 1000 runs were calculated for each iteration.

The simulation results for the same fronto-parallel example configuration and same initial points of the homography case are presented for the PnP methods in Fig. 5 and Fig. 6. For all the compared PnP methods the errors are reduced with iterations. The amount of improvement in EPnP and IPPE is stronger than for LM. The methods converge to similar error values along iterations. As seen in Fig. 6, not only the mean is reduced but also the variance, with a more pronounced effect on translation for the three methods. It is surprising that the point configuration also affects the performance of LM although our optimization objective is not directly related to the minimization of the reprojection error.

As a comparison, a simulation of an inclined camera pose (30 degrees to the $Z^P = 0$ plane) is presented with the same parameters as in the fronto-parallel case. The movements of the control points during the minimization process are presented in Fig. 7. The condition number and homography estimation error are presented in Fig. 8, and the results of the PnP estimation errors are presented in Fig. 9 and Fig. 10. As expected, the inclined case presents higher errors on the homography and pose estimation methods. The evolution of the condition number is also less smooth than in the fronto-parallel case which produces some large gradients during optimization and thus spikes in the homography error. This can be removed by finely tuning the SuperSAB parameters
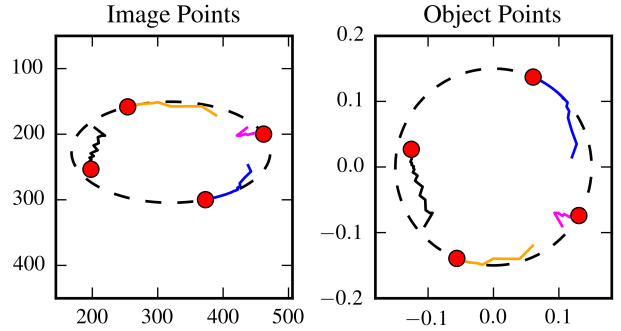
of the gradient descent for this particular case but the idea was to compare the simulation with the same parameters of the fronto-parallel case. The EPnP method has a large error with the initial point configuration which improves greatly with the optimization iterations. However, EPnP still has a large final error compared to IPPE and LM. The initial point configuration is also a difficult one for the LM an IPPE method but improves drastically with the optimization.

Next, a more profound study was performed. The same steps for simulating a single camera pose as presented in the fronto-parallel and inclined case were used for the total distribution of 400 camera poses shown in Fig. 2. For each pose 100 different initial random n-point configurations with $n \in \{4, 5, 6, 7, 8\}$ were simulated and the optimization process was performed until finding an optimal point configuration for each. In this case only the initial and final values of the point configuration metrics are stored. Thus, it is possible to compare the methods with *ill-conditioned* (inital points) and *well-conditioned* (after optimization) point configurations.
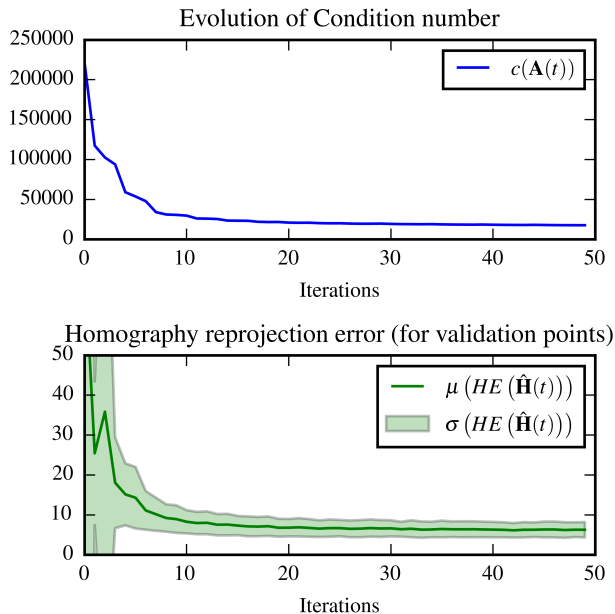
Fig. 8: (Inclined). Evolution of the condition number and the homography reprojection error during gradient descent.

Fig. 9: (Inclined). Comparison of the mean errors for the selected PnP estimation methods during the iterations of the optimization process.

In Fig. 11 the results for the homography estimation are presented and in Fig. 12 the results of the pose estimation. The median of the condition number was used instead of the mean since the mean presented high variation due to large particular cases. For the rest of the metrics the mean was selected. It can be seen, that the optimization process finds an optimal point configuration which on average is better for all the camera poses. Further on, the smaller the number of control points the more the optimization of the point configuration improves the homography estimate as well as the pose estimate for all of the evaluated methods. For example, the homography estimate using 4 optimal control points is always better than arbitrary point configurations with more points $4 < n \leq 9$. Choosing more than 4 optimal control points only slightly improves the homography estimates and converges for a number of 8 optimal control points. Thus, configuration of the control points clearly has much more effect on the accuracy than the number of control points. To verify that optimal 4-point configurations with maximal equal distance to each other has the biggest influence on the improvement of accuracy, we performed an additional test: A perfect square inscribed in the limits of the circular plane was selected as initial point configuration for all the camera poses and the metrics were calculated and compared with the results for optimal points obtained from the optimization process. For all of the poses, the square configuration has comparable performance than the optimal point configurations. The reason is because in most of the cases the shape of the final optimization points are also square-like. Thus, we verified that the corners of a square are almost optimal (if not optimal) control point configurations for space resection.
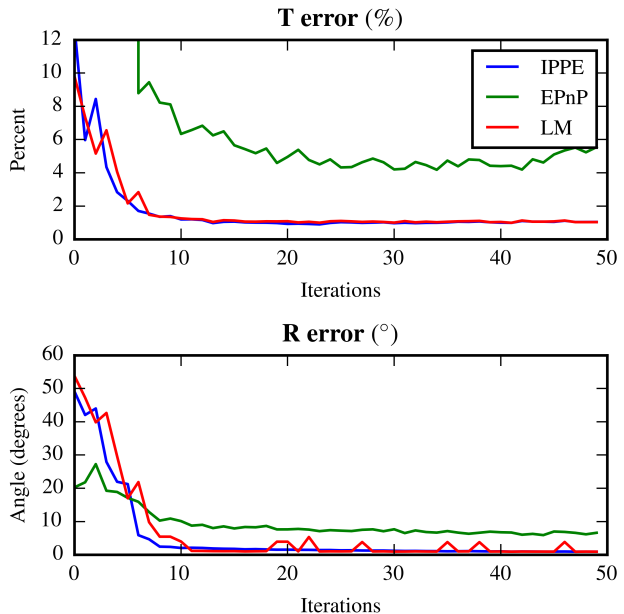
VI. Conclusions and future work

A method for obtaining optimal control points for homography estimation using an optimization approach is presented. It was shown that for a low amount of control points, the position of the points on the object plane have a strong influence on the accuracy of homography and PnP estimation methods. It was proven that a square is a very stable and robust configuration for all camera poses, which has been a common shape used in planar fiducial markers. For more point configurations the final shapes are not that well defined, however they meet the general rule of being maximally separated in object space with equal distances between each other including the optimal 4-point configuration as a subset. In future work, we will try to generalize the results to non-planar point configurations and head for real dynamic markers that optimize their control points within a visual servoing task.

References

[1] R. Hartley, "In defence of the 8-point algorithm," in *Proc. of IEEE Int. Conf. on Computer Vision*, 1997.

[2] P. Chen and D. Suter, "Error analysis in homography estimation by first order approximation tools: A general technique," *Journal of Mathematical Imaging and Vision*, 2009.

[3] E. Marchand, H. Uchiyama, and F. Spindler, "Pose Estimation for Augmented Reality: A Hands-On Survey," *IEEE Trans. on Vis. and Comput. Graphics*, 2016.

[4] D. Oberkampf, D. F. DeMenthon, and L. S. Davis, "Iterative Pose Estimation Using Coplanar Feature Points," *Computer Vision and Image Understanding*, 1996.

[5] C. P. Lu, G. D. Hager, and E. Mjolsness, "Fast and globally convergent pose estimation from video images," *IEEE Trans. Pattern Anal. Mach. Intell.*, 2000.

[6] V. Garro, F. Crosilla, and A. Fusiello, "Solving the PnP problem with anisotropic orthogonal procrustes analysis," *3DIMPVT*, 2012.
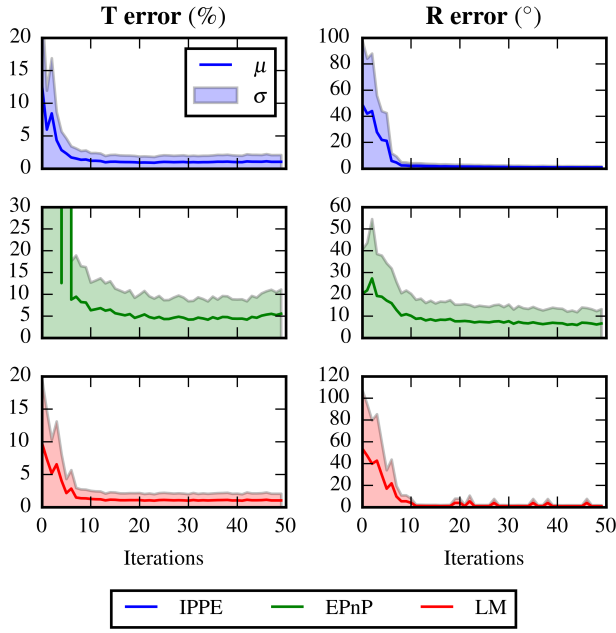
Fig. 10: (Inclined). Detailed view of the standard deviation of each method represented by the filled colored areas.
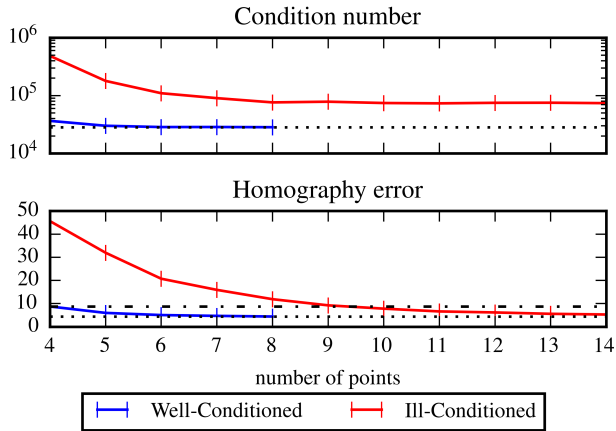

Fig. 11: Well-conditioned point configurations in contrast to ill-conditioned ones in homography estimation for different numbers of control points.
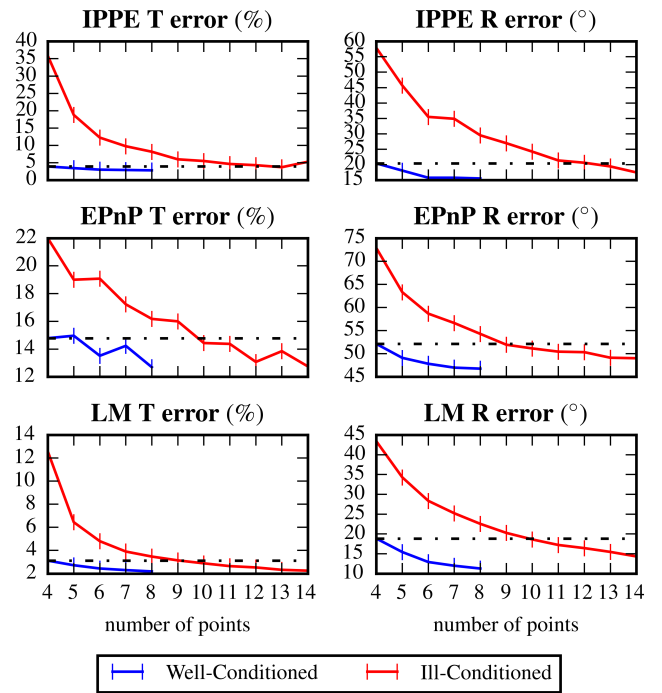

Fig. 12: Well-conditioned point configurations in contrast to ill-conditioned ones in pose estimation for different numbers of control points.

[7] G. Schweighofer and A. Pinz, "Globally Optimal O(n) Solution to the PnP Problem for General Camera Models," *BMVC*, 2008.

[8] V. Lepetit, F. Moreno-Noguer, and P. Fua, "EPnP: An accurate O(n) solution to the PnP problem," *International Journal of Computer Vision*, 2008.

[9] J. A. Hesch and S. I. Roumeliotis, "A direct least-squares (DLS) method for PnP," in *IEEE Int. Conf. on Computer Vision*, 2011.

[10] S. Li, C. Xu, and M. Xie, "A robust O(n) solution to the perspective-n-point problem," *IEEE Trans. Pattern Anal. Mach. Intell.*, 2012.

[11] Y. Zheng, Y. Kuang, S. Sugimoto, K. Astrom, and M. Okutomi, "Revisiting the PnP problem: A fast, general and optimal solution," in *Proc. of the IEEE Int. Conf. on Computer Vision*, 2013.

[12] L. Kneip, H. Li, and Y. Seo, "UPnP: An Optimal O(n) Solution to the Absolute Pose Problem with Universal Applicability," in *European Conference on Computer Vision*, 2014.

[13] G. Nakano, "Globally Optimal DLS Method for PnP Problem with Cayley parameterization," in *BMVC*, 2015.

[14] P. Sturm, P. Sturm, P.-b. P. Estimation, I. Conference, and P. Sturm, "Algorithms for Plane-Based Pose Estimation," *IEEE Conf. on Computer Vision and Pattern Recognition*, 2000.

[15] Z. Zhang, "A Flexible New Technique for Camera Calibration," *IEEE Trans. Pattern Anal. Mach. Intell.*, 2000.

[16] G. Schweighofer and A. Pinz, "Robust pose estimation from a planar target," *IEEE Trans. Pattern Anal. Mach. Intell.*, 2006.

[17] T. Collins and A. Bartoli, "Infinitesimal plane-based pose estimation," *International Journal of Computer Vision*, 2014.

[18] A. Z. Richard Hartley, *Multiple View Geometry*, 2nd ed. Cambridge University Press, 2004.

[19] M. J. Harker and P. L. O'Leary, "Computation of Homographies," in *BMVC*, 2005.

[20] P. Rangarajan and P. Papamichalis, "Estimating homographies without normalization," in *Proc. of Int. Conf. on Image Processing*, 2009.

[21] V. Willert, "Optical indoor positioning using a camera phone," in *Proc. of the 2010 int. conf. on indoor positioning and indoor navigation*, 2010.

[22] D. H. S. Chung, M. L. Parry, P. A. Legg, I. W. Griffiths, R. S. Laramee, and M. Chen, "Visualizing multiple error-sensitivity fields for single camera positioning," *Computing and Visualization in Science*, 2014.

[23] G. W. Stewart, "Perturbation theory for the singular value decomposition," Tech. Rep., 1998.

[24] G. H. Golub and C. F. Van Loan, *Matrix Computations*, 4th ed., 2013.

[25] D. Maclaurin, "Modeling, inference and optimization with composable differentiable procedures," Tech. Rep., 2016.

[26] L. B. Rall, "Automatic differentiation: Techniques and applications," 1981.

[27] T. Tollenaere, "Supersab: fast adaptive back propagation with good scaling properties," pp. Neural Networks 3(5), 561–573, 1990.